NANO LETTERS

2006
Vol. 6, No. 6
1131−1135

Carbon Nanotubes Encapsulating Superconducting Single-Crystalline Tin Nanowires

Luboš Jankovič,[†] Dimitrios Gournis,[*,†,‡] Pantelis N. Trikalitis,[*,§] Imad Arfaoui,[‡] Tristan Cren,[||] Petra Rudolf,[*,‡] Marie-Hélène Sage,[‡] Thomas T. M. Palstra,[‡] Bart Kooi,[‡] Jeff De Hosson,[⊥] Michael A. Karakassides,[†] Konstantinos Dimos,[†] Aliki Moukarika,[#] and Thomas Bakas[#]

Department of Materials Science and Engineering, University of Ioannina, 45110 Ioannina, Greece, Materials Science Centre, University of Groningen, Nijenborgh 4, 9747 AG, Groningen, The Netherlands, Department of Chemistry, University of Crete, 71409 Heraklion, Greece, Institut des Nanosciences de Paris, 140, rue Lourmel, 75015 Paris, France, Department of Applied Physics, Materials Science Centre, and the Netherlands Institute for Metals Research, University of Groningen, Nijenborgh 4, 9747 AG Groningen, The Netherlands, and Department of Physics, University of Ioannina, 45110 Ioannina, Greece

Received February 1, 2006; Revised Manuscript Received March 24, 2006

ABSTRACT

Superconducting low dimensional systems are the natural choice for fast and sensitive infrared detection, because of their quantum nature and the low-noise, cryogenic operation environment. On the other hand, monochromatic and coherent electron beams, emitted from superconductors and carbon-based nanostructured materials, respectively, are significant for the development of electron optical systems such as electron microscopes and electron-beam nanofabrication systems. Here we describe for the first time a simple method which yields carbon nanotubes encapsulating single crystalline superconducting tin nanowires by employing the catalytic chemical vapor deposition method over solid tin dioxide. The superconducting tin nanowires, with diameters 15–35 nm, are covered with well-graphitized carbon walls and show, due to their reduced diameters, a critical magnetic field (H_c) more than 30 times higher than the value of bulk metallic tin.

The hot-electron phenomena in low-dimensional superconducting systems are of fundamental importance for high energy resolution bolometers.[1] Photon absorption in a superconducting detector creates an avalanche electron charge, 2 or 3 orders of magnitude higher than that in a semiconductor for the same photon energy. This results in an enhanced resolution in energy-resolving devices, such as superconducting tunnel junctions,[2] and extends the range of detectable energies.[3] On the other hand, coherence of electron beams (e-beams) is of great interest for both practical and academic reasons since a highly coherent e-beam greatly improves the spatial resolution in electron optical systems.[4] In particular, the development of coherent e-beams with a high intensity will contribute to the further implementation of electron holography in practice.[5] In the pursuit of developing an ultracoherent e-beam, studies showed that the e-beam from a superconducting tip is monochromatic[6] and that e-beams emitted from different sites of a carbon nanotube can interfere with each other coherently.[7] For both applications the need of an easy and reproducible method to synthesize well-defined low-dimensional superconducting materials, easy to handle and at low cost, is of high importance. Superconducting nanowires and nanorods from lead,[8] tin,[9,10] and MoGe[11] have been already synthesized but are not suitable for handling since they are sensitive to oxidation. If such nanostructures can be protected and stabilized, they would be ideal to study the fundamental physical and chemical properties that are essential prior to their implementation as nano building blocks in nanoscale devices such as electron field emission sources or superconducting devices.

We report here a simple and reproducible method which yields individual micrometer-long carbon nanotubes filled

* To whom correspondence may be addressed. E-mail: dgourni@cc.uoi.gr; p.rudolf@rug.nl; ptrikal@chemistry.uoc.gr.
[†] Department of Materials Science and Engineering, University of Ioannina.
[‡] Materials Science Centre, University of Groningen.
[§] Department of Chemistry, University of Crete.
[||] Institut des Nanosciences de Paris.
[⊥] Department of Applied Physics, Materials Science Centre, and the Netherlands Institute for Metals Research, University of Groningen.
[#] Department of Physics, University of Ioannina.

10.1021/nl0602387 CCC: $33.50
Published on Web 05/03/2006

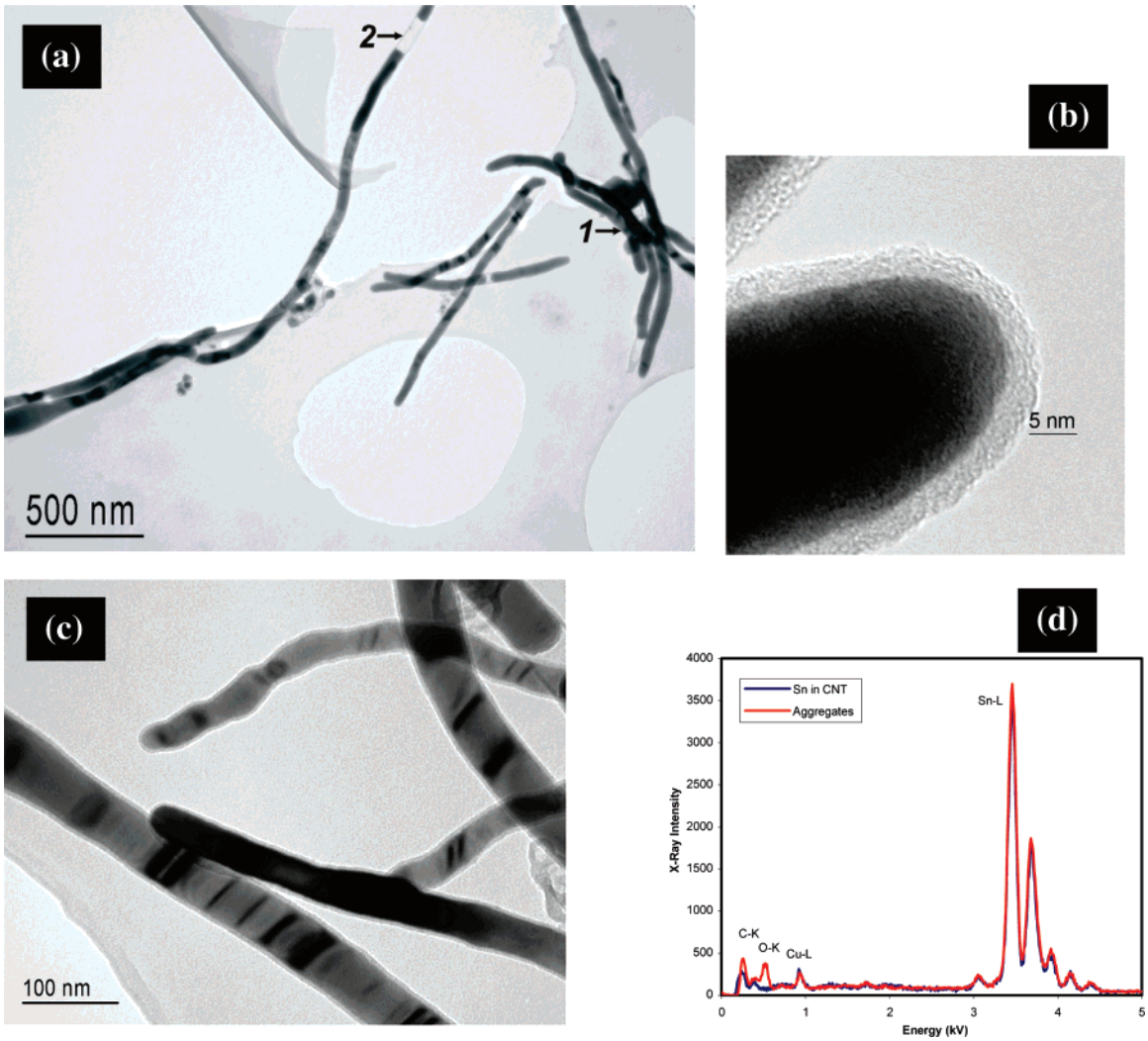

Figure 1. Low-magnification TEM images and EDXS spectra of Sn-CNT product, obtained by CCVD over solid SnO_2 using C_2H_2 as carbon source, showing the encapsulation of Sn nanowires. (a) Uniform MWCNTs, 20−40 nm wide and 4−5 μm long, are completely filled and encapsulate metallic Sn nanowires. Bundles of CNTs with amorphous carbon (mark 1) and few partially filled MWCNTs (mark 2) are also present. (b) All nanowires show apexes covered by carbon walls, making them suitable for handling in air. (c) The tin within the CNTs exhibits bending contour contrast. (d) Two EDS spectra: one taken with a relative small probe of 20 nm diameter on the Sn within a CNT, denoted as "Sn in CNT" (blue line); the other with a large diameter probe (about 500 nm) on aggregates of (partially) unreacted tin oxide and (amorphous) carbon in combination with the Sn-filled carbon nanotubes, denoted as "aggregates" (red line). The copper signal originates from the Cu grid.

with highly pure, single crystalline, superconducting tin nanowires. The novelty of our method, as compared to previous work,[10] is not only that it is a high yield, template-free, "one-pot" synthesis of free-standing tin nanowires but also more importantly that these nanowires are fully protected by carbon and hence totally inert in air. The surrounding carbon nanotube, consisting of only a few graphite layers, is closed in both ends thus protecting the nanowires. The superconducting tin nanowires show, due to their reduced diameters, a critical magnetic field (H_c) more than 30 times higher than the value of bulk metallic tin. The resulting composite nanostructure is denoted here as Sn-CNT.

Catalytic decomposition of acetylene at 700 °C over tin dioxide (see Materials and Methods in Supporting Information) produces Sn-CNT in high yield. The product of the reaction was investigated by transmission electron microscopy (TEM). Figure 1 shows the existence of uniform CNTs having encapsulated metallic nanowires. Most of the filled carbon nanotubes are isolated and not aggregated in bundles. However, bundles of nanotubes containing unreacted tin oxide and amorphous carbon are also observed (mark 1, Figure 1a). The filled carbon nanotubes (CNTs), whose diameters range between 20 and 40 nm, are up to 5 μm long and show a relatively uniform core (Figure 1a and Figure 1c). More than 90% of the tubes are fully filled with metallic tin; there are a few areas though (mark 2, Figure 1a) which are partially filled. Besides, all the observed endpoints (tips) of the tin nanowires are completely covered by carbon shells (Figure 1b). Therefore, the nanowires are protected from all sides against atmospheric oxidation and hence are suitable for handling in air. The tin within the CNTs often exhibits bending-contour contrast (see Figure 1c). Tilting of the samples shows movement of the dark and bright features of this contrast, indicating that this contrast does not originate

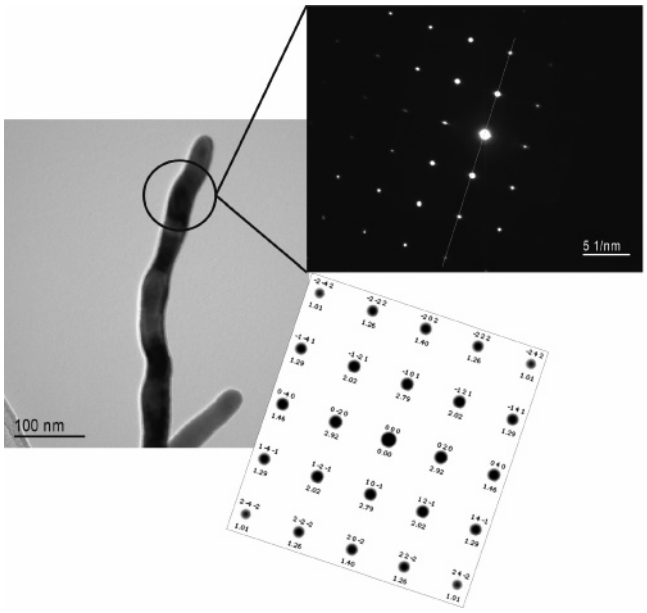

Figure 2. TEM image of a Sn full-filled CNT and the insets show the corresponding SAED patterns, experimental (top) and simulated (bottom), allowing to index this experimental pattern as metallic β-Sn as viewed along a ⟨101⟩ zone axis.

from localized defects (dislocations are ill-defined in these systems, twins are likely symmetrical twin boundaries and grown-in defects). Nevertheless, high-angle grain boundaries are in some instances present within the encapsulated Sn. It is logical that severe bending of the metallic tin is observed since the carbon nanotubes are far from straight.

With selected-area electron diffraction (SAED) and energy-dispersive X-ray spectrometry (EDS), tin oxide was not found within the CNTs. Figure 1d shows two EDS spectra; one taken with a probe of 20 nm diameter on the Sn within a CNT, denoted as "Sn in CNT" (blue line) in the figure, the other with a probe of about 500 nm on aggregates of (partially) unreacted tin oxide and (amorphous) carbon in combination with the Sn-filled carbon nanotubes, denoted as "aggregates" (red line) in the figure. Only the low-energy part up to 5 kV is shown, because it shows peaks of all the elements present. In the first spectrum no trace of an oxygen signal can be detected, whereas in the second spectrum an oxygen K-line is clearly present. Also, the carbon peak is somewhat more developed in the second spectrum because of the presence of (amorphous) carbon, not associated with filled carbon nanotubes. The copper signal originates from the Cu grid. Note that the small height of the carbon peak is also caused by absorption of the carbon signal by Sn. In fact, in the "Sn in CNT" spectrum the carbon signal only originates from the about 4 nm carbon on top of the tube, because the walls on the side were not part of the volume analyzed. Powder X-ray diffraction (XRD) in conjunction with ^{119}Sn Mössbauer spectroscopy illustrates the presence of β-Sn and SnO_2 phases in the final product (see Supporting Information). In the Mössbauer spectrum, obtained at 80 K, two quadrupole doublets were observed indicating the presence of these two Sn-containing phases. Analysis of the corresponding spectra shows that their relative percent ratio (SnO_2:β-Sn) is 0.59.

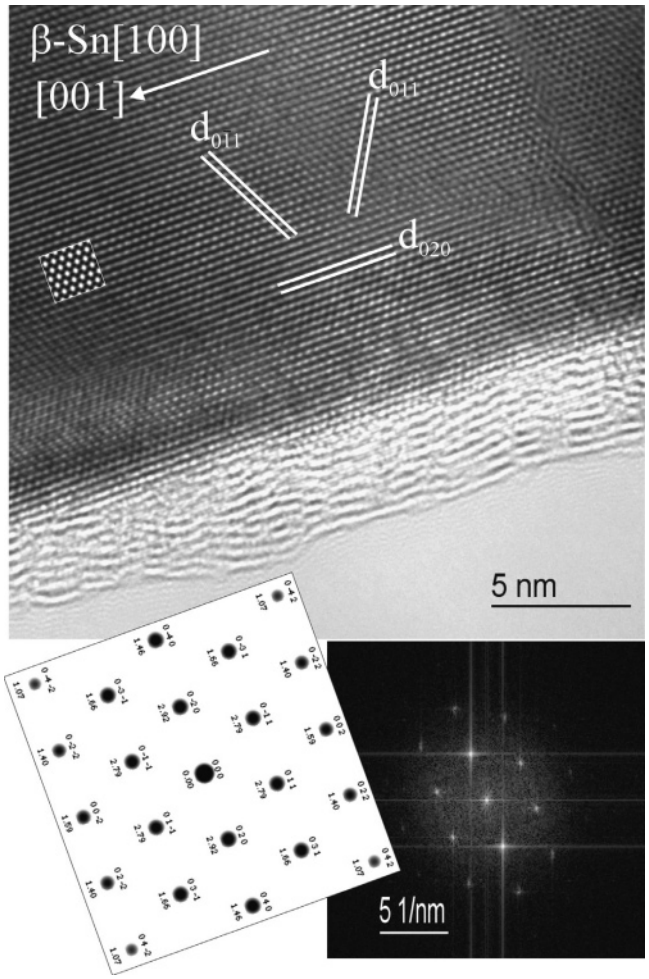

Figure 3. High-resolution TEM image showing the high degree of crystallinity of both the MWCNTs and the metallic tin nanowires. The preferential direction of growth is the ⟨001⟩ direction pointing more or less along the nanowire axis. The insets are the corresponding SAED patterns, experimental (right) and simulated (left) (an inset of the plane (001) of β-Sn is presented).

Unequivocal proof of the nature of the encapsulated phase within CNTs comes from SAED analysis. Figure 2 shows a typical SAED pattern that can be fully indexed as metallic β-Sn as viewed along a ⟨101⟩ zone axis. Moreover, the characteristic regular diffraction spots indicate that these are in fact single crystals. The crystals always extend the full width of the nanotubes and their length ranges from 50 nm to about 2 μm, with a most common length of about 1 μm. It is important to note here that in a large area of sample under TEM observation we did not observe any β-Sn phase outside the CNT. In other words, all the in situ formed β-Sn is encapsulated within CNTs in the form of long-range (up to several micrometers) single crystalline nanorods and tin dioxide was not found within the CNTs.

The high-resolution TEM images (Figure 3) show that the metallic tin nanowires are covered completely by a well-graphitized carbon layer. Typically around 10−12 carbon walls surround the tin. Additional information for the high degree of graphitization of the CNTs comes from Raman measurements (see Supporting Information). Comparing the present results with previous ones where tin nanowires

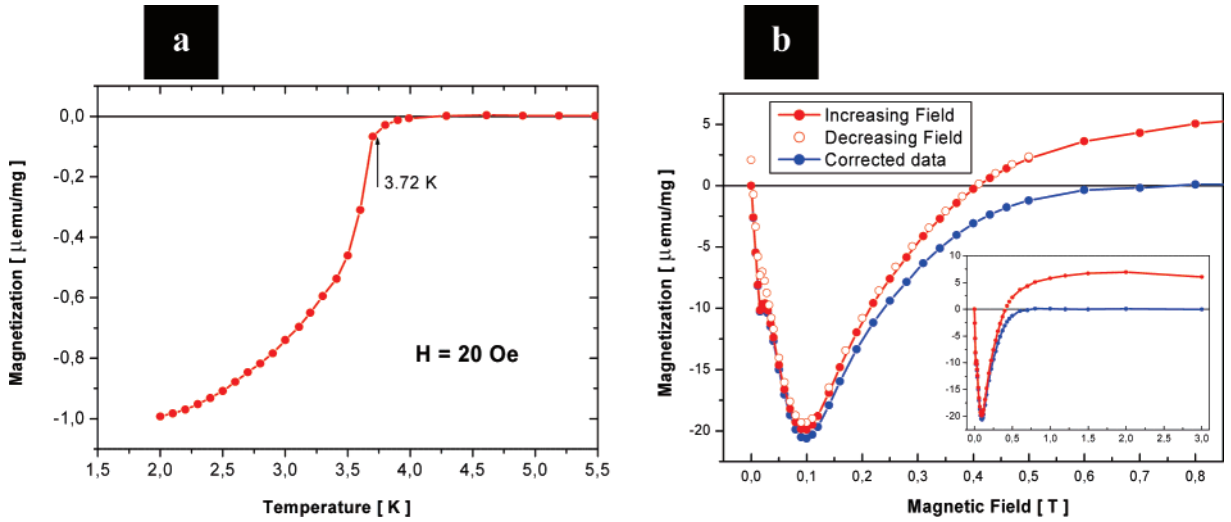

Figure 4. Superconducting properties of Sn-CNT product. (a) Magnetization versus temperature curve, taken at 20 Oe, showing a diamagnetic behavior below the bulk superconducting transition temperature for tin (indicated by the arrow). The small increase of the T_c onset is attributed to the thinnest tin nanowires present within the Sn-CNT product. (b) Magnetization versus magnetic field curve, taken at 2 K, showing a diamagnetic valley peaked around 0.1 T and, at high field ($H > 0.4$ T), the material becomes paramagnetic (see inset in Figure 4b). On removal of this paramagnetic background, the curve shows that the reduced diameter of the tin nanowires induces a huge increase of the critical field H_c in comparison with the bulk tin material.

(whiskers) were produced without the protecting CNTs[10,12] shows that the nanowires here are less straight and do not grow with a low-index crystal direction exactly along the nanowire axis. This difference can be understood since for noncovered nanowires the surface energy and facet formation play (during growth) a crucial role and will force the wire to have low energy facets along its long sides. In the present case the tin nanowires do not have a free surface but form noninteracting interfaces with the carbon. Moreover, the cross-sectional shape of the CNT is (nearly) round preventing the formation of low-energy facets. Nevertheless, in the present case still some preference was detected for growth with a ⟨101⟩ or ⟨001⟩ direction pointing more or less along the nanowire axis (Figure 3).

Since tin bulk material is a superconductor, magnetization measurements of Sn-CNT were carried out. Figure 4a shows the magnetization as a function of temperature for the Sn-CNT product measured with a field of 20 Oe. The data are normalized to the total mass of the powder which consists of carbon-encapsulated tin nanowires as well as small amounts of tin dioxide and amorphous carbon outside the tubes. The data show a clear diamagnetic behavior below the bulk superconducting transition temperature for tin $T_c =$ 3.72 K (indicated by the arrow).[10,12] The magnetization drops rapidly below the bulk T_c, but a small tail in the magnetization remains at temperatures as high as 4.0 K. As shown below, the small increase of the T_c onset is due to the thinnest nanowires in which the confinement and surface-to-volume ratio becomes large enough to influence the vibrational and electronic properties. The same has been reported in the literature[13] for tin nanowires of 20 nm diameter. Figure 4b shows the magnetization as a function of magnetic field at 2 K. The M vs H curve shows a diamagnetic valley peaked around 0.1 T. At high field ($H > 0.4$ T) the material becomes paramagnetic (see inset in Figure 4b). Without this paramagnetic background, the powder would still be diamagnetic at higher fields. This means that the onset of the superconducting critical field is higher than 0.4 T, which is more than 1 order of magnitude higher than the bulk thermodynamical critical field $H_c^{Bulk} = 0.021$ T at 2 K.[12] Measurements above T_c show that the apparent paramagnetic background is in fact the sum of a temperature-dependent paramagnetic signal, probably due to a few magnetic impurities, superimposed to a temperature-independent diamagnetic contribution. A simple removal of the background is shown in Figure 4b (black circles) where we see that the onset of critical field is of the order of 0.6 T. This increase in the critical field is a direct result of the reduced diameter of the nanowires.[9,10,14] The ultrapure tin nanowires are in the clean limit of the microscopic BCS theory, where the mean free path, l, is longer than the coherence length ξ ($l \gg \xi$). In such a case, a nanocylinder of radius R smaller than the coherence length $R < \xi$ and with a magnetic field applied along its axis has a critical field $H_c = \exp(3/2)\Phi_0/\pi^2\xi R$, where $\Phi_0 = h/2e$ is the quantum of flux.[14] Thus, the thinnest wires have a strongly enhanced critical field. The field penetrates completely through such thin wires, and the Meissner effect is strongly reduced. Consequently, the demagnetizing field is also suppressed. Hence, we expect the critical field to be almost independent of the orientation of the field. With these assumptions, and taking a BCS coherence length of $\xi(2\text{ K}) \cong 250$ nm,[15] we find that the onset critical field of 0.6 T corresponds to tin nanowires of 13 nm in diameter. This order of magnitude for the thinner nanowires is in agreement with the HRTEM images. Note that the nanowires have a large size dispersion since we also observe a small jump in the magnetization around H_c^{Bulk}, which is due to nanowires with a diameter larger than ξ. These few big tin rods are also responsible for the very small hysteresis of the $M(H)$ curve (see Figure 4b). At fields higher than H_c^{Bulk} the hysteresis is negligible; hence nanowires of diameter much smaller than ξ cannot pin the magnetic flux.

In wires with diameters smaller than 20 nm, confinement effects are no longer negligible since the transverse level spacing $\delta\epsilon = \hbar^2/m^*2R^2$ exceeds the superconducting pairing energy Δ (the formation of a Cooper pair induces an energy gain of 2Δ). Hence, the quantization of both electron and phonon energy could modify the effective electron−phonon interaction responsible for the superconductivity.[9,16] In particular, the density of states on the energy scale Δ becomes spiky, and this leads to fluctuations in the amplitude of the order parameter.[14] For the thinnest wires, this effect is expected to enhance the critical temperature T_c.[14] This could explain why the T_c onset is higher than the bulk T_c. This enhancement could also be attributed to an increase of the electron−phonon coupling resulting from the decrease of the phonon frequencies and the influence of surface−phonon modes.[17]

In conclusion, we have demonstrated a simple and reproducible method which yields carbon nanotubes encapsulating single-crystalline, superconducting tin nanowires. The diameter of the metal core is in the range of 15−35 nm, and the walls consist of cylindrical graphene sheets, 5 nm thick, parallel to the tube axis. Although the mechanism of the tin filled CNT growth is under investigation, it is expected that a microcapillarity phenomenon is taking place since at the reaction temperature of 700 °C β-Sn is liquid. Such behavior has been reported recently in other low-melting metal incorporated in CNTs.[18] However, the mechanism of the CNT growth remains to be explored. Magnetization measurements show a slight increase in the superconducting temperature and a considerable increase (more than 30 times) of the critical magnetic field ($H_c = 0.6$ T) compared to bulk metallic tin (0.021 T). These materials might be useful as functional components and interconnects in future electronic and superconducting nanodevices or as nanosensors.

Acknowledgment. This work was performed within the EU RT network CassiusClays Contract No. HPRN-CT-2002-00178 and received additional support from the FOM (The Netherlands). This research was supported in part by the Rijksuniversiteit Groningen's Breedtestrategie program and by the MSC*plus* program. The authors would like to acknowledge the use of the XRD unit of the Laboratory Network, UoI.

Note Added after ASAP Publication. This article was published ASAP on May 3, 2006. Figure 4 y-axis labels were corrected. The revised version was reposted on May 5, 2006.

Supporting Information Available: Materials and methods, powder X-ray diffraction data, and ^{119}Sn Mössbauer and Raman spectra. This material is available free of charge via the Internet at http://pubs.acs.org.

References

(1) Alessandrello, A.; Beeman, J. W.; Brofferio, C.; Cremonesi, O.; Fiorini, E.; Giuliani, A.; Haller, E. E.; Monfardini, A.; Nucciotti, A.; Pavan, M.; Pessina, G.; Previtali, E.; Zanotti, L. *Phys. Rev. Lett.* **1999**, *82*, 513; Gol'tsman, G. N.; Okunev, O.; Chulkova, G.; Lipatov, A.; Semenov, A.; Smirnov, K.; Voronov, B.; Dzardanov, A.; Williams, C.; Sobolewski, R. *Appl. Phys. Lett.* **2001**, *79*, 705.
(2) Peacock, A.; Verhoeve, P.; Rando, N.; vanDordrecht, A.; Taylor, B. G.; Erd, C.; Perryman, M. A. C.; Venn, R.; Howlett, J.; Goldie, D. J.; Lumley, J.; Wallis, M. *Nature* **1996**, *381*, 135.
(3) Il'in, K. S.; Milostnaya, II.; Verevkin, A. A.; Gol'tsman, G. N.; Gershenzon, E. M.; Sobolewski, R. *Appl. Phys. Lett.* **1998**, *73*, 3938.
(4) Cho, B.; Ogawa, T.; Ichimura, T.; Ichinokawa, T.; Amakusa, T.; Oshima, C. *Rev. Sci. Instrum.* **2004**, *75*, 3091.
(5) de Hosson, J. T. M.; de Raedt, H. A. Nano-structured thin films: a Lorentz transmission electron microscopy and electron holography study. In *Pricm 5: the Fifth Pacific Rim International Conference on Advanced Materials and Processing*, Pts 1−5, 2005; Vol. 475−479; p 4241.
(6) Nagaoka, K.; Yamashita, T.; Uchiyama, S.; Yamada, M.; Fujii, H.; Oshima, C. *Nature* **1998**, *396*, 557.
(7) Oshima, C.; Mastuda, K.; Kona, T.; Mogami, Y.; Komaki, M.; Murata, Y.; Yamashita, T.; Kuzumaki, T.; Horiike, Y. *Phys. Rev. Lett.* **2002**, *88*, 038301.
(8) Vodolazov, D. Y.; Peeters, F. M.; Piraux, L.; Matefi-Tempfli, S.; Michotte, S. *Phys. Rev. Lett.* **2003**, *91*, 157001; Zhang, Y.; Dai, H. J. *Appl. Phys. Lett.* **2000**, *77*, 3015.
(9) Hsu, Y. J.; Lu, S. Y. *J. Phys. Chem. B* **2005**, *109*, 4398.
(10) Tian, M. L.; Wang, J. G.; Snyder, J.; Kurtz, J.; Liu, Y.; Schiffer, P.; Mallouk, T. E.; Chan, M. H. W. *Appl. Phys. Lett*. **2003**, *83*, 1620.
(11) Bezryadin, A.; Lau, C. N.; Tinkham, M. *Nature* **2000**, *404*, 971; Lau, C. N.; Markovic, N.; Bockrath, M.; Bezryadin, A.; Tinkham, M. *Phys. Rev. Lett.* **2001**, *87*, 217003.
(12) Natsik, V. D.; Soldatov, V. P.; Ivanchenko, L. G.; Kirichenko, G. I. *Low Temp. Phys.* **2004**, *30*, 253.
(13) Tian, M. L.; Wang, J. G.; Kurtz, J. S.; Liu, Y.; Chan, M. H. W.; Mayer, T. S.; Mallouk, T. E. *Phys. Rev. B* **2005**, *71*, 104521.
(14) Han, J. E.; Crespi, V. H. *Phys. Rev. B* **2004**, *69*, 214526.
(15) Orlando, T. P.; Delin, K. A. *Foundations of Applied Superconductivity*; Addison-Wesley: Reading, MA, 1991.
(16) Guo, Y.; Zhang, Y. F.; Bao, X. Y.; Han, T. Z.; Tang, Z.; Zhang, L. X.; Zhu, W. G.; Wang, E. G.; Niu, Q.; Qiu, Z. Q.; Jia, J. F.; Zhao, Z. X.; Xue, Q. K. *Science* **2004**, *306*, 1915. Hwang, E. H.; Das Sarma, S.; Stroscio, M. A. *Phys. Rev. B* **2000**, *61*, 8659. Paskin, A.; Singh, A. D. *Phys. Rev.* **1965**, *140*, 1965.
(17) Leger, A.; Klein, J. *Phys. Lett. A* **1969**, *28*, 751. Strongin, M.; Kammerer, O. F.; Crow, J. E.; Parks, R. D.; Douglass, D. H.; Jensen, M. A. *Phys. Rev. Lett.* **1968**, *21*, 1320.
(18) Chen, J. Y.; Kutana, A.; Collier, C. P.; Giapis, K. P. *Science* **2005**, *310*, 1480. Gao, Y. H.; Bando, Y. *Nature* **2002**, *415*, 599.

NL0602387